Synthesis and photoluminescence properties of Eu^{3+}-doped ZrO_2 hollow spheres

Min Zhang
College of Materials Science and Engineering, Beijing Institute of Petrochemical Technology, Beijing, Beijing 102617, China

Weiwei Zuo[a] and Meifang Zhu
State Key Laboratory for Modification of Chemical Fibers and Polymer Materials, Donghua University, Shanghai, Shanghai 201260, China

Dianguang Liu,[b] Yigao Chen, Meng Zhu, Haoran Hong, Chengyu Yang, and Yiguang Wang[c]
State Key Laboratory of Solidification Processing, Northwestern Polytechnical University, Xi'an, Shanxi 710072, China

Jinling Liu
State Key Laboratory of Traction Power, School of Mechanics and Engineering, Southwest Jiaotong University, Chengdu, Sichuan 610031, China

Linan An
Department of Materials Science and Engineering, Advanced Materials Processing and Analysis Center, University of Central Florida, Orlando, Florida 32816, USA

(Received 30 September 2015; accepted 23 November 2015)

ZrO_2:Eu^{3+} hollow spheres were successfully fabricated with the resin microspheres as the template. The sample characterizations were carried out by means of x-ray diffraction (XRD), scanning electron microscope (SEM), and photoluminescence spectra. XRD results revealed that Eu^{3+}-doped samples were pure t-ZrO_2 phase after being calcined at 873 K. SEM results exhibited that this Eu^{3+} doped ZrO_2 was hollow spheres; the diameter and thickness of which were about 450 and 50 nm, respectively. Upon excitation at 394 nm, the orange-red emission bands at the wave length longer than 570 nm were from $^5D_0 \rightarrow {}^7F_J$ (J = 1, 2) transitions. The asymmetry ratio of ($^5D_0 \rightarrow {}^7F_2$)/($^5D_0 \rightarrow {}^7F_1$) intensity is about 1.61, 1.26, 1.42, 1.42, 1.40, and 1.38 for the Eu^{3+} concentration 0.4, 0.7, 1.0, 1.5, 2.0, and 2.5 mol%, respectively. These values suggest that the asymmetry ratio of Eu^{3+} ions is independent of the doping concentration. The optimal doping concentration of Eu^{3+} ions in ZrO_2 is 1.5 mol%. According to Dexter's theory, the critical distance between Eu^{3+} ions for energy transfer was determined to be 16 Å.

I. INTRODUCTION

Rare earth (RE) ion-doped materials have drawn great attention due to their significant technological importance and are used as solid state lighting, medical labeling, imaging, radiation detection, and other functional compounds based on their optical, electronic, and chemical characteristics.[1–6] The macroscopic properties of phosphors, such as the emission spectrum or the luminous efficiency, rely on their composition, crystal structure, and morphology.[7–12] Extensive work has been devoted to the development of effective morphology-controlled methods to synthesize functional materials with complex three-dimensional (3D) hierarchical architectures, such as Fe_2O_3 flower-like microspheres,[13] urchin-like WO_3 and $MnWO_4$ microstructures,[14,15] cactus-like β-Ga_2O_3 microarchitectures,[16] dandelion-like ZnO and CuO architectures,[17,18] 3D hierarchical MWO_4 (M = Mn, Bi, Ba, and Pb), and $MMoO_4$ (M = Fe, Pb, and Ba) superstructures,[9,19–23] which have been fabricated from low dimensional nanobuilding units by bottom-up approaches. Since sphere morphology of phosphor is favorable for high brightness and high resolution, spherical structured particles have been interestingly studied in these years.[16–18]

The selection of host materials for RE ions is crucial to obtain large luminescence signals.[14] Materials with low phonon energies present small nonradiative losses owing to the multiphonon relaxation, and consequently, the luminescence efficiency is enhanced. A suitable host must also present large optical band gap along with good solubility and stability. Zirconia is a suitable host for RE material because it offers a large transparency window from the short ultraviolet to the near infrared frequencies and has excellent mechanical properties and good chemical

Contributing Editor: Xiaobo Chen
Address all correspondence to these authors.
[a]e-mail: zuoweiwei@dhu.edu.cn
[b]Co-first author
[c]e-mail: wangyiguang@nwpu.edu.cn
DOI: 10.1557/jmr.2015.375

stability.[15] Generally speaking, the luminescence properties of phosphors strongly depend on the physical properties, such as specific surface area, crystallinity, particle size, size distribution, and morphology, of their host materials. To understand the detailed factors controlling the luminescence and to find the better ways to enhance the photoluminescence (PL) property, for instance, a lot of efforts related to photoluminescence of nanometer zirconia powders based on different synthetic methods have been made.[24–27] To the best of our knowledge, there are few reports related to Eu^{3+}-doped ZrO_2 hollow nanospheres, which were exploited for photoluminescence properties.

Herein, we provide a facile and effective route for shape-controlled synthesis of ZrO_2:Eu^{3+} hollow spheres with the help of phenolic resin microspheres as template. The luminescence properties were studied in detail and PL spectra indicated that the ZrO_2:Eu^{3+} particles presented excellent orange-red emission at 614 nm and excited at 394 nm. The effects of doped content and critical distance of Eu^{3+} ions in the ZrO_2 have been systematically explored.

II. EXPERIMENTAL

A. Synthesis of hollow sphere ZrO_2:Eu^{3+}

All the reagents are of the analytical grade. The phenolic resin microspheres with diameter around 400 nm were synthesized according to literature.[28–30] As shown in Scheme 1, a typical synthesis of the hollow sphere ZrO_2:Eu^{3+} with 500 nm diameter was synthesized as following procedures. 6.7 mmol of $ZrClO_2{\cdot}8H_2O$ aqueous solution (20 mL) was mixed with a solution (20 mL) containing 0.78 mmol of $Y(NO_3)_3{\cdot}6H_2O$, 1.6 mmol of citric acid, and 0.2 g of the template, phenolic resin microspheres. Subsequently, different amounts of $Eu(NO_3)_3{\cdot}6H_2O$ (0.4%, 0.7%, 1.0%, 1.5%, 2.0%, and 2.5 mol%) aqueous solution were added and continually stirred for 30 min, respectively. 0.03 g of polyvinylpyridine (PVP) and 0.2 g of urea were then added to the reaction solution and stirred for 5 h. The ZrO_2/phenolic resin composite microsphere-doped Eu^{3+} was recovered by centrifugation and air-dried at 100 °C for 12 h. For the sintering, the powder was heated under air atmosphere to 600 °C with a heating rate of 1 °C min^{-1}, then maintained at 600 °C for 2 h before measurements.

B. Characterization

The crystal structure of the samples was identified by x-ray diffractometer (Rigaku D/max-2400, Tokyo, Japan). Their diffraction patterns were obtained using Cu K_α radiation of wave length $\lambda = 0.15418$ nm. The morphology of the powder was recorded by a field-emission scanning electron microscope (SEM, S-4700; Hitachi, Tokyo, Japan). The room temperature PL, photoluminescence excitation (PLE) spectra, and decay curves of the products were measured by a fluorescence spectrophotometer (Hitachi F-4600, Tokyo, Japan) with a 450-W xenon lamp. In all experiments, both excitation and emission slits were 1.0 nm.

III. RESULTS AND DISCUSSION

A. Crystallization behavior and morphology

X-ray diffraction (XRD) analysis of ZrO_2:Eu^{3+} products sintered at 873 K for 2 h was used to identify the sample phase and was shown in Fig. 1. The XRD pattern indicates that all the ZrO_2:Eu^{3+} precursors underwent thermal transformation to ZrO_2:Eu^{3+} samples and formed pure t-ZrO_2 (JCPDS 50-1089) phase with good crystallization. No other phase was found because the template of the resin microspheres could be oxidized at high temperature.

The morphology of ZrO_2:Eu^{3+} (1.5 mol%) powders prepared under the above mentioned conditions was studied by the SEM under different magnifications. Figure 2(a) shows that the templates, composed of phenolic resin microspheres, are regular spherical particles with uniform size about 400–500 nm. Figure 2(b) exhibited ZrO_2-covered template spheres with slightly increased diameter of 500–600 nm. Seen from Figs. 2(c) and 2(d), after postheated at 873 K for 2 h, the as-synthesized ZrO_2:Eu^{3+} was hollow sphere with the diameter and the thickness of about 450 nm and the 50 nm, respectively.

B. Luminescence properties of ZrO_2:Eu^{3+}

Due to the similarities in PLE and PL spectra of the samples with different Eu^{3+} concentrations, typical spectra of ZrO_2 with 0.4 mol% Eu^{3+} content are shown in the Fig. 3. The PLE spectrum monitored at 614 nm presents a series of intraconfiguratioal 4f-4f transitions of

SCHEME 1. Schematic illustration of the formation process of ZrO_2:Eu^{3+} hollow spheres.

Eu^{3+} as follows: $^5D_4$(362 nm), $^5G_4$(383 nm), and $^5L_6$(394 nm) of Eu^{3+} ions, respectively.[7] These transitions are followed by subsequent population decay to $^5D_0$ luminescent excited state. With excitation at 394 nm, two main PL bands, associated with the 4f-4f internal orbital transitions of Eu^{3+} ions, are clearly resolved. They can be related to the radiative transitions from the $^5D_0$ state to ^7F_J (J = 1, 2) states of Eu^{3+} at 594 and 614 nm, respectively.

Figure 4 shows the PL spectra of ZrO_2:Eu^{3+} synthesized at 873 K for 2 h with different doping concentrations of Eu^{3+} (0.4, 0.7, 1.0, 1.5, 2.0, and 2.5 mol%) and the comparison with pure ZrO_2:Eu^{3+} powder. Upon excitation at 394 nm, the orange-red emission bands at the wave length longer than 570 nm are from $^5D_0 \rightarrow {}^7F_J$ (J = 1, 2) transitions. The $^5D_0 \rightarrow {}^7F_1$ band centered at 594 nm (orange) is a magnetic dipole transition and hardly varies with the crystal field strength around the Eu^{3+} ion. On the other hand, the hypersensitive transition $^5D_0 \rightarrow {}^7F_2$ at 614 nm (red) is electric dipole allowed. Consequently, it depends on the local electric field, and hence, the local symmetry influences its strength. From these considerations, the ($^5D_0 \rightarrow {}^7F_2$)/($^5D_0 \rightarrow {}^7F_1$) intensity ratio gives a measure of the degree of distortion from the inversion symmetry of Eu^{3+} ion local environment. The asymmetry ratio is about 1.61, 1.26, 1.42, 1.42, 1.40, and 1.38, which correspond to the Eu^{3+} concentration 0.4, 0.7, 1.0, 1.5, 2.0, and 2.5 mol%, respectively. These different values suggest that the

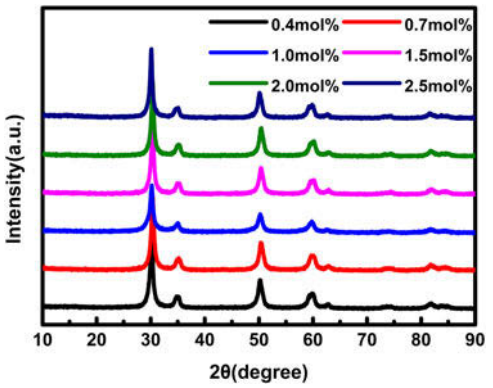

FIG. 1. The XRD patterns of the as-synthesized Eu^{3+}-doped samples postannealed at 873 K with different doping concentrations of Eu^{3+} (0.4, 0.7, 1.0, 1.5, 2.0, and 2.5 mol%).

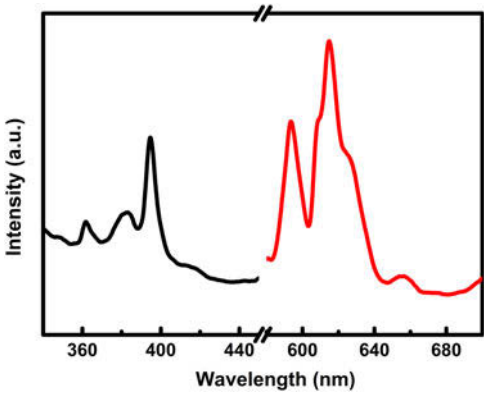

FIG. 3. Excitation and emission spectra of ZrO_2:Eu^{3+} (0.4 mol%) powder calcined at 873 K for 2 h.

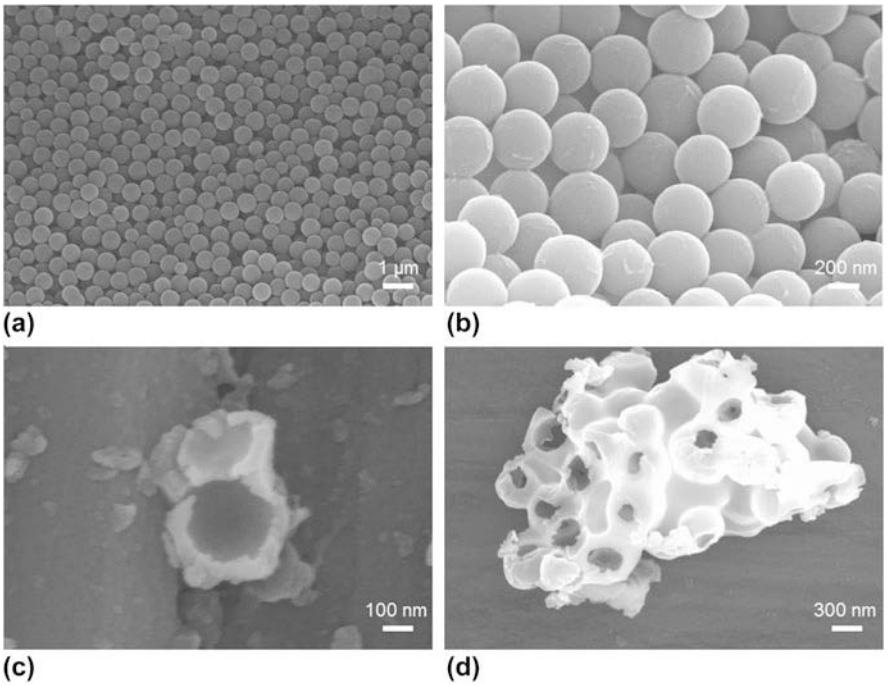

FIG. 2. SEM images of the products before (a and b) and after (c and d) postheated at 873 K for 2 h under different magnifications.

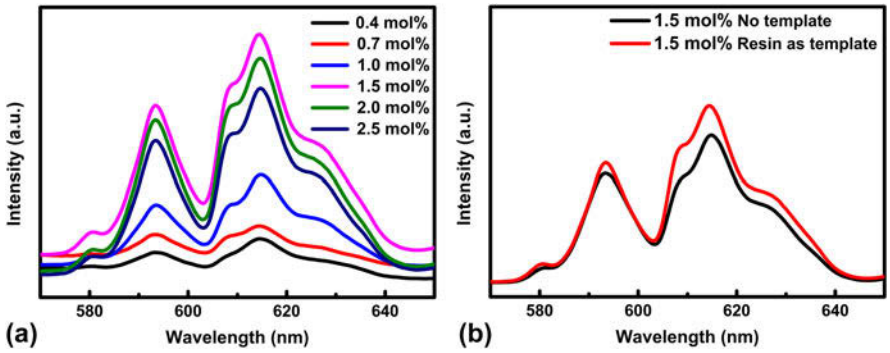

FIG. 4. Emission spectra of ZrO_2:Eu^{3+}: (a) the samples synthesized at 873 K for 2 h with different doping concentrations of Eu^{3+} (0.4, 0.7, 1.0, 1.5, 2.0, and 2.5 mol%); (b) comparison of ZrO_2:Eu^{3+} hollow sphere emission spectra with pure ZrO_2:Eu^{3+} powder.

asymmetry ratio of Eu^{3+} ions were independent of the doping concentration. In addition, it is evident that the emission intensity depends on the doping concentration. At low Eu^{3+} concentrations ($\chi < 1.5$ mol%), the emission intensity is weak because there are no sufficient luminescence centers. However, under the condition of increasing Eu^{3+} concentration, the emission intensity increases and reaches the maximal value at 1.5 mol%. When the Eu^{3+} doping ratio is greater than 1.5 mol%, the luminescence intensity starts to reduce as concentration quenching occurs due to the decrease in Eu–Eu distance.[20] Based on Dexter's theory,[21] the critical distance between Eu^{3+} ions for energy transfer can be calculated by the following relation:

$$R_c \approx [6V/\pi x_c Z]^{1/3} \quad , \qquad (1)$$

where V is the volume of the unit cell, x_c is the critical concentration of the doping ions, and Z is the number of host cation in the unit cell. For t-ZrO_2, $V = 66.7$ Å^3, $Z = 2$, and the critical concentration of Eu^{3+} in the ZrO_2 host is 0.015. Therefore, the R_c of Eu^{3+} ions is determined to be 16 Å. What is more, the luminescence intensity of ZrO_2:Eu^{3+} hollow sphere and pure ZrO_2:Eu^{3+} powder was compared, which was shown in Fig. 4(b). Obviously, the luminescence intensity of ZrO_2:Eu^{3+} hollow sphere was stronger than pure ZrO_2:Eu^{3+} powder.

PL decay curves of ZrO_2: Eu^{3+} with different concentrations of Eu^{3+} (0.4, 0.7, 1.0, 1.5, 2.0, and 2.5 mol%), shown in Fig. 5, were used to calculate the lifetime and investigate the luminescence dynamics of the samples. The samples were excited at 394 nm and monitored at 614 nm, and the curves were obtained with fluorescence spectrophotometer under Time Scan mode, and the lifetime values were calculated by the software of the spectrophotometer (Fluorescence Solutions for F-4600). It is found that the curves followed the single-exponential decay

$$I_t = I_0 \exp(-t/\tau) \quad , \qquad (2)$$

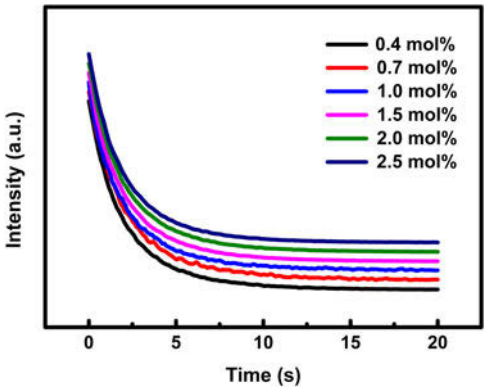

FIG. 5. The decay curves of ZrO_2:Eu^{3+} phosphors synthesized at 873 K for 2 h with different concentrations of Eu^{3+} (0.4, 0.7, 1.0, 1.5, 2.0, and 2.5 mol%).

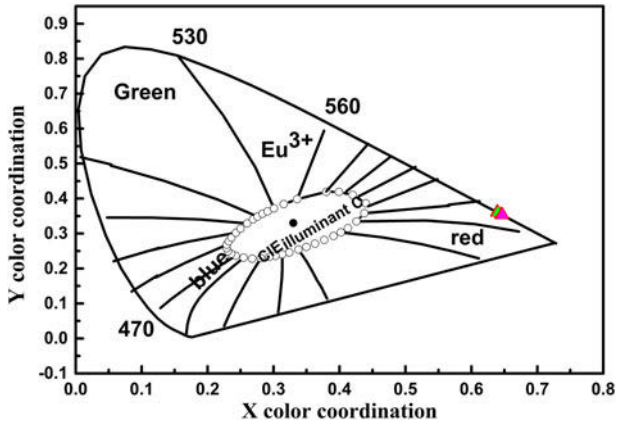

FIG. 6. The Commission Internationale de L'Eclairage (CIE) coordinates of ZrO_2:Eu^{3+} phosphors synthesized at 873 K for 2 h with different concentrations of Eu^{3+} (0.4, 0.7, 1.0, 1.5, 2.0, and 2.5 mol%).

where I_t is the intensity at time t, I_0 is the intensity at $t = 0$, and τ is the decay lifetime. The fitted fluorescence lifetime values of ZrO_2: Eu^{3+} are 3.43, 3.5, 3.42, 3.36, 3.45, and 3.35 ms corresponding to the Eu^{3+} concentration 0.4, 0.7, 1.0, 1.5, 2.0, and 2.5 mol%, respectively. The single-exponential decay curve reveals that these

bands are not related to the defects of Eu host matrix, which is also confirmed by Podhorodecki.[22]

The color coordinates for the orange-red emission in the present experiment are calculated based on the corresponding PL spectra, and the results are shown in Fig. 6. The coordinates (x, y) of ZrO_2:Eu^{3+} are (0.645, 0.354), (0.639, 0.361), (0.640, 0.360), (0.646, 0.353), (0.646, 0.353), and (0.647, 0.353), which correspond to the Eu^{3+} concentration 0.4, 0.7, 1.0, 1.5, 2.0, and 2.5 mol%, respectively. These results indicate that the as-obtained phosphors could show merits of orange-red emissions in the visible region when excited by a single wave length light, which might find potential applications in the fields such as light display systems and optoelectronic devices.[23]

IV. CONCLUSION

In summary, the controllable generation of ZrO_2:Eu^{3+} hollow spherers has been successfully achieved with the resin microspheres as the template. The diameter and thickness of the samples were about 450 and 50 nm, respectively. Upon excitation at 394 nm, the orange-red emission bands at the wave length longer than 570 nm are from $^5D_0 \rightarrow {}^7F_J$ (J = 1, 2) transitions. The asymmetry ratio is about 1.61, 1.26, 1.42, 1.42, 1.40, and 1.38, which correspond to the Eu^{3+} concentration 0.4, 0.7, 1.0, 1.5, 2.0, and 2.5 mol%, respectively. These different values suggest that the asymmetry ratio of Eu^{3+} ions was independent of the doping concentration. From the luminescence study, the optimum concentration of luminescence is found to be 1.5 mol%. The critical energy transfer distance of Eu^{3+} in t-ZrO_2 host is calculated to be 16 Å. The single-exponential decay curves reveal that these bands do not relate to the defects of Eu host matrix. Because of the suitable excitation band, controllable morphology, good CIE chromaticity, and chemical stability, the luminescence materials may find potential applications in fields such as optoelectronic and nanoscale devices or biological technology.

ACKNOWLEDGMENT

This work was financially supported by the National Natural Science Foundation of China under Grant Nos. 21404084 and 51532003, the foundation of State Key Laboratory for Modification of Chemical Fibers and Polymer Materials (Donghua University), the Fundamental Research Funds for the Central Universities under Grant No. B040307 and the funding from the State Key Laboratory of Solidification Processing in NWPU (Grant No. 107-QP-2014) and the 111 Project (B08040).

REFERENCES

1. K. Riwotzki, H. Meyssamy, and H. Schnablegger: Liquid-Phase Synthesis of Colloids and Redispersible Powders of Strongly Luminescing $LaPO_4^-$:Ce,Tb Nanocrystals., Angew. *Angew. Chem. Int. Ed.* **40**, 573–576 (2001).
2. S. Sudhahar, M.K. Kumar, V. Jayaramakrishnan, R. Muralidharan, and R.M. Kumar: Effect of Sm^+ Rare Earth Ion on the Structural, Thermal, Mechanical and Optical Properties of Potassium Hydrogen Phthalate Single Crystals. *J. Mater. Sci. Technol.* **30**, 13–18 (2014).
3. W.X. Wang, Z.Y. Cheng, and P.P. Yang: Patterning of YVO_4:Eu^{3+} Luminescent Films by Soft Lithography. *Adv. Funct. Mater.* **21**, 456–463 (2011).
4. E.H. Penilla, Y. Kodera, and J.E. Garay: Blue–Green Emission in Terbium-Doped Alumina (Tb:Al_2O_3) Transparent Ceramics. *Adv. Funct. Mater.* **23**, 6036–6043 (2013).
5. J. Joo, T. Yu, and Y.W. Kim: Multigram scale synthesis and characterization of monodisperse tetragonal zirconia nanocrystals. *J. Am. Chem. Soc.* **125**, 6553–6557 (2003).
6. X.J. Liang, B.F. Liu, and N. Chen: Growth and Photoluminescence Properties of Tetrapod-Shaped ZnO Microcrystals-Whiskers and Microrods. *J. Mater. Sci. Technol.* **25**, 427–432 (2009).
7. D.G. Liu and Z.F. Zhu: Photoluminescence properties of the Eu-doped alpha-Al_2O_3 microspheres. *J. Alloys Compd.* **583**, 291–294 (2014).
8. M.M. Rahman, M.K.R. Khan, M.R. Islam, M.A. Halim, M. Shahjahan, M.A. Hakim, D.K. Saha, and J.U. Khan: Effect of Al Doping on Structural, Electrical, Optical and Photoluminescence Properties of Nano-Structural ZnO Thin Films. *J. Mater. Sci. Technol.* **28**, 329–335 (2012).
9. D.G. Liu: Effects of Cr content and morphology on the luminescence properties of the Cr-doped alpha-Al_2O_3 powders. *Ceram. Int.* **39**, 4765–4769 (2013).
10. D. Boyer and R. Mahiou: Powders and Coatings of $LiYF_4$:Eu^{3+} Obtained via an Original Way Based on the Sol–Gel Process. *Chem. Mater.* **16**, 2518–2521 (2004).
11. Z. Deng, X.D. Pi, J.J. Zhao, and D. Yang: Photoluminescence from Silicon Nanocrystals in Encapsulating Materials. *J. Mater. Sci. Technol.* **29**, 221–224 (2013).
12. C.J. Jia, L.D. Sun, and L.P. You: Selective Synthesis of Monazite- and Zircon-type $LaVO_4$ Nanocrystals. *J. Phys. Chem. B* **109**, 3284–3290 (2005).
13. Q. Chen, Y.Q. Chang, C.J. Shao, J. Zhang, J. Chen, M.W. Wang, and Y. Long: Effect of Grain Size on Phase Transformation and Photoluminescence Property of the Nanocrystalline ZrO_2 Powders Prepared by Sol-Gel Method. *J. Mater. Sci. Technol.* **30**, 1103–1107 (2014).
14. L.X. Yu, H.W. Song, and S.Z. Lu: Luminescent Properties of $LaPO_4$:Eu Nanoparticles and Nanowires. *J. Phys. Chem. B* **108**, 16697–16702 (2004).
15. N. Rakov and G.S. Maciel: Enhancement of luminescence efficiency of f–f transitions from Tb^{3+} due to energy transfer from Ce^{3+} in Al_2O_3 crystalline ceramic powders prepared by low temperature direct combustion synthesis. *Chem. Phys. Lett.* **400**, 553–557 (2004).
16. Q.H. Fan, P. Li, Z. Zheng, W.S. Wu, and C.L. Liu: Insights into sorption species of Eu(III) on γ-Al_2O_3 and bentonite under different pH: Studies at macro- and micro-scales. *J. Radioanal. Nucl. Chem.* **299**, 1767–1775 (2014).
17. X.Y. Xu, Y.X. Liu, Z. Lv, J.Q. Song, M.Y. He, Q. Wang, L.J. Yan, and Z.F. Li: Thermal study in Eu^{3+}-doped boehmite nanofibers and luminescence properties of the corresponding Eu^{3+}:Al_2O_3. *J. Therm. Anal. Calorim.* **118**, 1585–1592 (2014).
18. G.G. Li, C. Peng, and C.X. Li: Shape-controllable synthesis and morphology-dependent luminescence properties of GaOOH:Dy^{3+} and beta-Ga_2O_3:Dy^{3+}. *Inorg. Chem.* **49**, 1449–1457 (2010).
19. G. Jia, Y.J. Huang, and Y.H. Song: Controllable Synthesis and Luminescence Properties of $La(OH)_3$ and $La(OH)_3$:Tb^{3+} Nanocrystals

with Multiform Morphologies. *Eur. J. Inorg. Chem.* **2009**, 3721−3726 (2009).
20. G. Blasse and B.C. Grabmaier: *Luminescent Materials* (Springer, Berlin, 1994).
21. G. Blasse: Energy Transfer in Oxidic Phosphors. *Philips Res. Rep.* **24**, 131−143 (1969).
22. A. Podhorodecki, M. Banski, J. Misiewicz, and J. Serafińczuk: Influence of Annealing on Excitation of Terbium Luminescence in $YAlO_3$ Films Deposited onto Porous Anodic Alumina Semiconductor Devices, Materials, and Processing. *J. Electrochem. Soc.* **157**, H628 (2010).
23. N.V. Gaponenko, I.S. Molchan, O.V. Sergeev, and G.E. Thompson: Enhancement of Green Terbium-Related Photoluminescence from Highly Doped Microporous Alumina Xerogels in Mesoporous Anodic Aluminasensors and Displays: Principles, Materials, and Processing. *J. Electrochem. Soc.* **149**, H49 (2002).
24. Q. Li, D. Ai, X. Dai, and J. Wang: Photoluminescence of nanometer zirconia powders. *Powder Technol.* **137**, 34−40 (2003).
25. W. Du, Z. Zhu, X. Zhang, D. Wang, D. Liu, X. Qian, and J. Du: RE/ZrO_2 (RE = *Sm*, *Eu*) composite oxide nano-materials: Synthesis and applications in photocatalysis. *Mater. Res. Bull.* **48**, 3735–3742 (2013).
26. R. Marin, G. Sponchia, E. Zucchetta, P. Riello, G. De Portu, F. Enrichi, and A. Benedetti: Monitoring the $t \rightarrow m$ Martensitic Phase Transformation by Photoluminescence Emission in Eu^{3+}-Doped Zirconia Powders. *J. Am. Ceram. Soc.* **96**, 2628–2635 (2013).
27. X. Gao, D. He, H. Jiao, J. Chen, and X. Meng: Fabrication of $SiO_2@ZrO_2@Y_2O_3:Eu^{3+}$ Core-Multi-Shell Structured Phosphor. *J. Nanosci. Nanotechnol.* **8**, 6963–6968 (2011).
28. J. Liu, S. Qiao, H. Liu, J. Chen, A. Orpe, D. Zhao, and G. Lu: Extension of the Stöber Method to the Preparation of Monodisperse Resorcinol–Formaldehyde Resin Polymer and Carbon Spheres. *Angew. Chem.* **123**, 6069–6073 (2011).
29. D. Chen, J. Liu, P. Wang, L. Zhang, J. Ren, F. Tang, and W. Wu: Fabrication of monodisperse zirconia-coated core–shell and hollow spheres in mixed solvents. *Colloids Surf., A* **302**, 461–466 (2007).
30. F. Lin, W. Dong, C. Liu, Z. Liu, and M. Li: In situ source–template-interface reaction route to hollow ZrO_2 microspheres with mesoporous shells. *J. Colloid Interface Sci.* **323**, 365–371 (2008).